Electron-donating strength dependent symmetry breaking charge transfer dynamics of quadrupolar molecules

ARTICLE

Electron-Donating Strength Dependent Symmetry Breaking Charge Transfer Dynamics of Quadrupolar Molecules

Received 00th January 20xx,
Accepted 00th January 20xx

DOI: 10.1039/x0xx00000x

Xinmiao Niu, [a, b, †] Zhuoran Kuang,[a,b, †] Miquel Planells,[c] Yuanyuan Guo, [a,b] Neil Robertson,*[c] Andong Xia*[a,b]

The excited state symmetry breaking charge transfer (SBCT) dynamics of two diacetylide-triphenylamine (DATPA) derivatives with different electron-donating abilities are investigated by femtosecond transient absorption and fluorescence spectroscopy. By tracking the evolution of the excited states by transient absorption spectra and the kinetics of the instantaneous emission dipole moments obtained from transient fluorescence spectroscopy, it is found that, in nonpolar solvent, the relaxed S_1 state is quadrupolar with little change of emission dipole moments for the two molecules within 30 ps; whereas in polar solvent, the quadrupolar state evolves to a symmetry broken S_1 state, in which, the emission dipole moment exhibits a fast reduction in the first few picoseconds. The larger reduction in emission transition dipole moment for the molecule with stronger electron-donating methoxy groups indicates a larger extent of symmetry breaking compared with the one with weak electron-donating methyl groups. Consequently, we revealed that the magnitude of symmetry breaking can be tuned by changing the electron-donors in quadrupolar molecules.

Introduction

Intramolecular charge transfer (ICT) is one of the most fundamental and ubiquitous chemical reactions in organic molecules which contain electron-donor (D) and -acceptor (A) units.[1-6] The property of ICT has been proven to play a critical role in energy conversion and storage processes in photovoltaics, organic light emitting diodes (OLED) and nonlinear optics.[7-15] The ICT process, which takes place readily in dipolar molecules, is easily influenced by the polarity of the surrounding environments, and leads to fluorescence solvatochromism or a decrease in fluorescence quantum yield along with an increase in static dipole moment in the excited state.[16-18] When ICT occurs in molecules with D-π-A-π-D or A-π-D-π-A quadrupolar, or D-π-A_3, A-π-D_3 octupolar symmetry structures,[19-25] their ground-state absorption usually presents little solvent dependence because of symmetry characteristics but emission shows a strong solvatochromism effect, indicative of quadrupolar or octupolar ground state but dipolar emission state.[26-34] This phenomenon was rationally interpreted by symmetry breaking charge transfer (SBCT), which is triggered by the fluctuation of molecular structure upon photoexcitation or the local field generated by the surrounding solvents.[35-38]

Over the past few years, a lot of studies have examined the role of the surrounding solvents in the SBCT processes, and the results show that the extent of symmetry breaking is controlled by the interaction between the solute and solvent.[35, 39] For quadrupolar molecules upon photoexcitation, the electronic excitation distributes evenly on the two branches. While in case of symmetry breaking, electronic distribution partially localizes on the one of the two branches,[40] leading to an excited state with some dipolar character. Understanding the influence of the nature of the solute molecule itself on the extent of symmetry breaking is, however, uncommon to compare for the above-mentioned themes. Therefore, we present a study of the amplitude of symmetry breaking modulated by the different electron-donating strength groups in different polar solvents. We chose two quadrupolar molecules with different electron-donating functional groups, 4,4'-(buta-1,3-diyne-1,4-diyl)bis(*N*,*N*-di-*p*-tolylaniline) and 4,4'-(buta-1,3-diyne-1,4-diyl)bis(*N*,*N*-bis(4-methoxyphenyl)aniline) (molecular structures shown in Figure 1), which are comprised of two triphenylamine moieties (TPA) linked with a diacetylene group. The TPA moieties with strong electron-donating ability are regarded as donors and the diacetylene groups with weak electron-withdrawing property are regarded as acceptors.[41] The two molecules differ only in the peripheral substituents with different electron-donating abilities. One molecule contains two methyl groups, named as **Me-DATPA**, and the other features two methoxy groups, named as **MeO-DATPA** (Figure 1). The methoxy substituent possesses a stronger electron-donating ability than the methyl group, hence it is expected that

[a.] *Beijing National Laboratory for Molecular Sciences (BNLMS), Key laboratory of Photochemistry, Institute of Chemistry, Chinese Academy of Sciences, Beijing 100190, People's Republic of China. E-mail: andong@iccas.ac.cn*
[b.] *University of Chinese Academy of Sciences, Beijing 100049, People's Republic of China.*
[c.] *EastChem – School of Chemistry, University of Edinburgh, Kings Buildings, Edinburgh EH9 3JJ, UK. E-mail: neil.robertson@ed.ac.uk*
† These authors contributed equally.
Electronic Supplementary Information (ESI) available: [Experiments details, photophysical parameters, TCSPC and nanosecond TA data, additional TA, TF data, fitting qualities of TA spectra, and detail data analysis of TF data]. See DOI: 10.1039/x0xx00000x

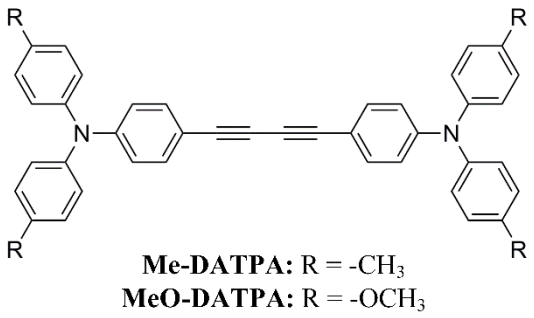

Figure 1. Molecular structures of **DATPA** derivatives.

MeO-DATPA will experience a stronger ICT than **Me-DATPA**, reflected on SBCT dynamics.[41]

The SBCT dynamics can be tracked in real-time by time-resolved spectroscopic experiments. Time-resolved infrared spectroscopy is the most direct technique by monitoring the specific vibrational modes located at the two branches of the quadrupolar molecules while it may not be adequate for molecules without ideal infrared markers.[42] Although the C≡C bond in our case is a typical infrared marker, the central two directly linked C≡C bonds in the **DATPA** derivatives are expected to share almost the same electronic excitation even if symmetry breaking has occurred in the excited state, leading to a difficult identification in infrared spectra. Time-resolved transient absorption (TA) spectroscopy can track the evolution of the excited electronic state in the SBCT process and further deduce the structural dynamics, but it does not provide a direct evidence of SBCT. Recently, Vauthey and Kim presented an approach to trace the instantaneous transition emission dipole moment (μ_{em}) by femtosecond time-resolved transient fluorescence (TF) spectroscopy, providing direct evidence of the SBCT processes.[29, 42, 43] Therefore we present an investigation using two time-resolved spectroscopic measurements (femtosecond TA and TF measurements) to detect the SBCT dynamics of the two **DATPA** derivatives. The combination of the two methods not only directly tracks the SBCT process in real-time, but also yields a deeper insight into the excited electronic state dynamics. In addition, quantum chemical calculation using combined density functional theory (DFT) and time-dependent DFT (TD-DFT) was employed, which has become a completely reliable tool to analysis the properties of the ground state and the vertical absorption spectra.[44-47] The results show that both molecules experience a SBCT process in the excited states in polar THF. As expected, **MeO-DATPA,** which has the stronger electron-donating functional group methoxy, was found to has a larger extent of symmetry breaking compared with the **Me-** analogue. In other words, the extent of SBCT increases as the stronger electron-donating ability of the substitute in the quadrupolar molecule.

Materials and methods

Materials

The synthesis and structural characterization of **Me-DATPA** and **MeO-DATPA** were described elsewhere.[41] All aprotic solvents used for spectroscopic measurements were analytical grade and without further purification.

Steady-state measurements

Steady-state absorption spectral measurements were conducted on a U-3010 (Hitachi) spectrophotometer, and fluorescence spectral measurements were carried out on an F-4600 (Hitachi) fluorescence spectrophotometer. Quartz cuvettes with 1-cm optical path length were used in steady-state spectral measurements. Fluorescence quantum yields (FQYs) were measured by a comparison method with 9,10-diphenylanthracene as a standard reference (FQY = 0.9 in cyclohexane, excited at 370 nm).[48] Fluorescence lifetimes were measured with time-correlated single photon counting (TCSPC) technique, excited by a picosecond LED source (PLS-500, PicoQuant) at 370 nm with FWHM of ~400 ps.

Transient spectral measurements

Femtosecond TA spectra were performed using a home-built broadband pump-probe system and the apparatus is described in detail in Section S1.[49, 50] Sample solutions were prepared in 1-mm thick quartz cuvettes with the absorbance ~0.3 OD at 400 nm. Glotaran software based on R-package TIMP was used to analyze the obtained femtosecond TA data.[51, 52] Nanosecond TA measurements were performed on an LP920 laser flash photolysis spectrometer (Edinburgh Instruments Ltd), excited at 355nm by a Nd:YAG laser (Surelite II, Continuum Inc.). Sample solutions were excited at 355 nm with the absorbance values of 0.3 OD at 355 nm in quartz cuvettes with 1-cm optical path length. Femtosecond TF spectra were conducted on a commercial TF spectrometer (FluoMax-MP, IB Photonics) based on femtosecond fluorescence up-conversion technique, and the details are also described in Section S1. The transition emission dipole moment (μ_{em}) is also calculated as shown in SI (Section S2).[43]

Quantum calculation details

All calculations were implemented in Gaussian 09 software package.[53] The geometrical optimizations for the ground state were performed using density functional theory at CAM-B3LYP/6-31G(d) level. CAM-B3LYP has been proven to have a good performance in prediction of vibrational frequencies and charge transfer transition.[54, 55] Vibrational frequencies were calculated based on the optimized structures to prove the minimum energy geometry. Time-dependent density functional theory was used to calculate the vertical transition energies at the same level and basis set based on the optimized ground state structures.[56] The calculation results are in agreement with the observed spectra, indicating the rationality of these calculation methods used in our work.

Results and discussion

Photophysical properties

Figure 2 shows the steady-state absorption and fluorescence spectra of **Me-DATPA** and **MeO-DATPA** in solvents with

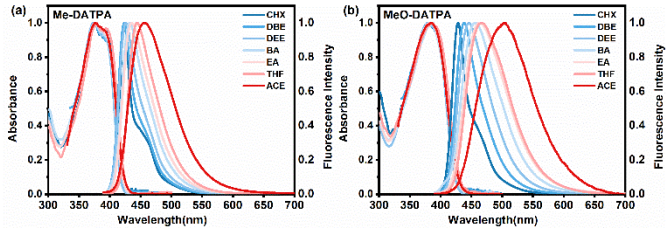

Figure 2. Normalized steady-state absorption and fluorescence spectra of **Me-DATPA** and **MeO-DATPA** in different polar solvents. (CHX, cyclohexane; DBE, di-n-butyl Ether; DEE, diethyl ether; BA, butyl acetate; EA, ethyl acetate; THF, tetrahydrofuran; ACE, acetone).

different polarity, the detailed spectral parameters in various solvents are listed in Table S2. The absorption band for the two molecules with the maximum at ~380 nm is ascribed to charge transfer transition, as evidenced by quantum chemical calculations (Section S3). The absorption spectra are broader than emission spectra, and there is no obvious mirror-image symmetry relationship in nonpolar CHX which can be explained by the conformation difference between ground- and excited-states. The conformation exhibits a trend of planarization in S_1 relative to S_0, suggesting a trend of enhanced conjugation from the optimized S_0 state to S_1 state. [57] It is found that the positions of absorption bands of the two molecules are not significantly affected by the solvent polarity because of small dipole moments, which is consistent with the quadrupolar properties of ground states. The different electron-donating group has a negligible effect on the absorption spectra, whereas it has a great impact on the fluorescence solvatochromism behaviours. From nonpolar cyclohexane (CHX, $\Delta f = 0$) to strongly polar acetone (ACE, $\Delta f = 0.285$), the fluorescence bands of **Me-** and **MeO-DATPA** downshift by 2455 cm^{-1} and 3586 cm^{-1}, respectively. A plot of the emission maximum against the solvent orientation polarizability $\Delta f = \frac{(\varepsilon-1)}{(2\varepsilon+1)} - \frac{(n^2-1)}{(2n^2+1)}$, where ε is the dielectric constant and n is the refractive index,[58] was performed as shown in Figure S2 and Table S3. It is found that the slope of **MeO-DATPA** in nonpolar to medium solvents is steeper than that for **Me-DATPA**, and becomes significantly enhanced in strong polar solvents. This indicates the permanent dipole moment of the relaxed S_1 state changes with the solvent polarity, suggesting the broken symmetry of the relaxed S_1 state.[59] The larger solvatochromism of **MeO-DATPA** indicates that the stronger electron-donating effect can enhance a stronger dipolar character for the S_1 state in more polar solvents.

According to the fluorescence quantum yields and fluorescence lifetimes measurements (see Table S4 and Figure S3 in SI), the fluorescence quantum yields and radiative rate constants of the two molecules decrease along with the increased solvent polarity. This is a typical characteristic of solvation effects, indicating the emission state in polar solvent is an asymmetric charge transfer state. Although the two molecules exhibit the same trend, the decline in fluorescence intensity and k_r are more prominent for **MeO-DATPA** than that for **Me-DATPA**. This suggests that **MeO-DATPA** undergoes a stronger dipole-dipole interaction in solvation and exhibits a larger dipolar character in the relaxed S_1 state compared to **Me-DATPA**.

Table 1 shows the calculated emission dipole moments of the relaxed S_1 states for the two molecules in CHX and THF. The magnitude of emission dipole moment for **Me-DATPA** is estimated to be ~11.5 D in CHX and ~8.2 D in THF, while for **MeO-DATPA**, the value is ~11.1 D in CHX and ~5.5 D in THF, respectively. The decreased emission dipole moment in THF indicates that the nature of the emission state has been changed.[29, 42] Under the increased solvent polarity, both molecules lose their quadrupolar symmetry and appear like dipolar molecules. The relaxed emissive S_1 state in THF could be a SBCT state while the symmetry is maintained in nonpolar CHX. It is also worth noting that the larger decline in emission dipole moment for **MeO-DATPA** compared with **Me-DATPA** points to a larger extent of symmetry breaking in THF. To obtain insight into the dynamics of the symmetry breaking processes, fs-TA and fs-TF measurements were performed.

Femtosecond TA spectra

Femtosecond TA spectra were measured for the two molecules in CHX and THF as shown in Figure 3. TA spectra of both **Me-DATPA** and **MeO-DATPA** in CHX show similar features. Following the photoexcitation at 400 nm, two main features are observed. A negative feature centred around 455 nm is ascribed to the stimulated emission (SE), in agreement with the major peak of the steady-state fluorescence spectrum. The sharp positive signal centred at 660 nm related to excited-state absorption (ESA) band was observed, where the intensity of ESA band increases during the first tens of picoseconds, which is linked to a conformational planarization followed with the formation of the vibrational-related structural relaxation of the S_1 state.[60] Afterward, the overall spectral intensity decays slowly with a negligible spectral shape change during the following time delays.

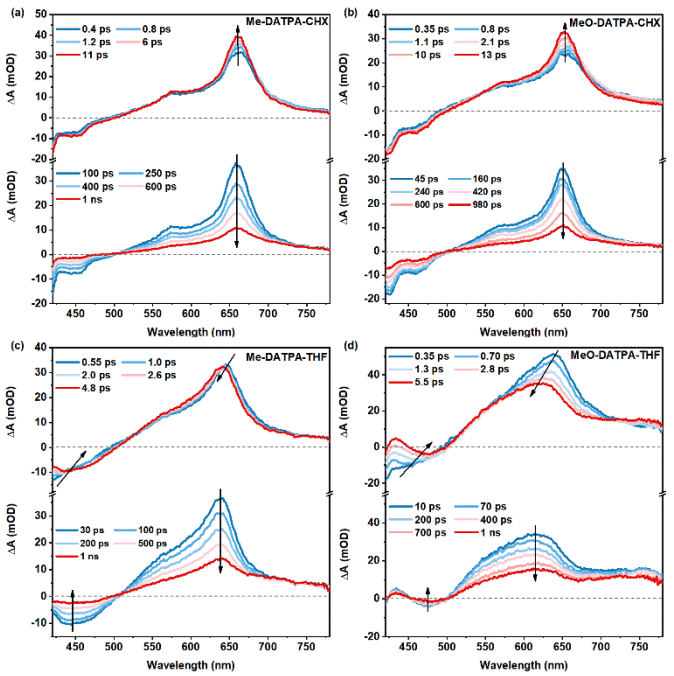

Figure 3. Femtosecond TA spectra of **Me-DATPA** (a), **MeO-DATPA** (b) in CHX and **Me-DATPA** (c), **MeO-DATPA** (d) in THF.

Table 1. Dynamic parameters obtained by the target analysis of **Me-DATPA** and **MeO-DATPA** in CHX and THF.

	solvent	τ_1 (ps)	τ_2 (ns)	τ_{ISC} (ns)	τ_{em}-dipole[a] (ps)	μ_{em} in FC[b] (D)	μ_{em} in relaxed S_1[c] (D)
Me-DATPA	CHX	15.5 ± 0.2	~0.66	~2.6	/	12.1	11.5
	THF	3.2 ± 0.2	~1.2	~1.	2.6 ± 0.1	9.6	8.2
MeO-DATPA	CHX	21 ± 0.4	~0.82	~1.9	/	11.6	11.1
	THF	2.8 ± 0.1	~1.6	~3.7	2.8 ± 0.15	8.2	5.5

[a] $\tau_{em\text{-}dipole}$ is the time constant obtained by fitting the dynamic of emission dipole moment.

[b] μ_{em} in FC state is calculated from transient fluorescence spectra in 0.2 ps.

[c] μ_{em} in relaxed S_1 state is calculated from steady-state fluorescence spectra.

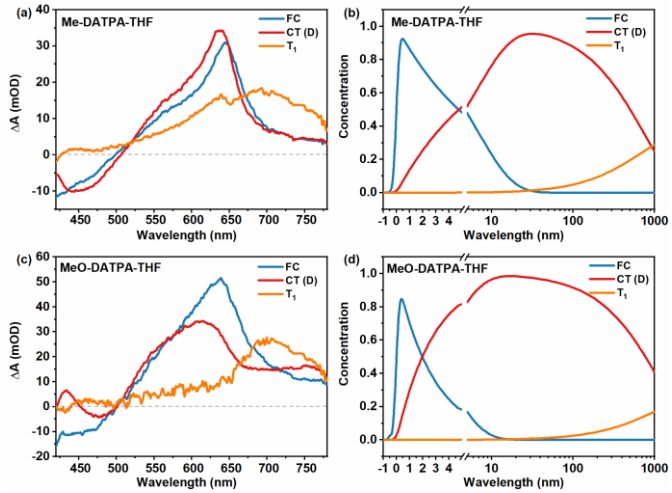

Figure 4. SADSs from target analysis of **Me-DATPA** (a) and **MeO-DATPA** (c) in THF. Concentration evolution of transient species of **Me-DATPA** (b) and **MeO-DATPA** (d) in THF.

In THF, the fs-TA spectra show substantial differences compared with those recorded in CHX. For **Me-DATPA,** the negative band with the maximum at ~440 nm is ascribed to SE corresponding to the stationary fluorescence, and positive signal associated with ESA centred around 645 nm was observed as well. The initial SE band slightly red-shifts with a concomitant blue shift of the ESA within ~8 ps. The red-shift of SE band is characteristic of a solvation-induced conformation stabilizing process of a CT state.[49, 61] During this process the symmetry breaking of the initial quadrupolar state may take place. Over a longer timescale, SE and ESA bands decay simultaneously over the whole wavelength region, indicating a fully relaxed emissive S_1 which should contain the SBCT character observed in stationary photophysical study.[27] For **MeO-DATPA**, the initial TA spectrum contains a SE peaked around 460 nm and an ESA with a narrow band at 640 nm. The SE band rapidly red-shifts from 460 nm to 480 nm, and in the meantime, the ESA band blue-shifts and evolves into a broader band, which reflects a more pronounced solvent-induced conformation relaxation in the emissive S_1. The different magnitudes of red-shifts of SE bands for the two molecules indicate that different strength electron-donor obviously affects the nature of the excited state.

To analyse the underlying mechanism in the excited state, we performed global spectral analysis with a target model. Three-time constants (Figure 8) are required for the best fitting of the TA spectra of the two molecules. The fitting results are shown in Table 1 and Figure 4, as well in Figure S4 and S5 (see ESI). For each molecule in CHX, photoexcitation at 400 nm directly excites the molecules up to the upper vibrational energy levels of the singlet state with their ground-state quadrupolar symmetry, so the first species-associated difference spectra (SADS) is ascribed to the Frank-Condon (FC) state. The second SADS shows the similar spectral feature with the first SADS, except the increased intensity of ESA band relative to the first SADS. Accordingly, the two SADSs stand for two relaxation stages for the quadrupolar state, the rise is contributed to a conformational planarization followed with the formation of the vibrational-related structural relaxation in the S_1 state. And therefore, τ_1 is assigned to the time of conformational relaxation and τ_2 is the lifetime of the relaxed quadrupolar state. The third SADS exhibits an entirely different features from the former two, with two ESA bands at 640 nm and 680 nm, which are similar to the spectra of the triplet state obtained by the nanosecond transient spectra (shown in Section S7), thus can be assigned to the ESA of T_1 state and τ_3 is the time constant of intersystem crossing. For the two molecules in THF, a similar proposed model is used in target analysis, giving three SADSs corresponding to FC state, the solvent-induced conformational relaxed state and T_1 state. Therefore, τ_1 is attributed to the time

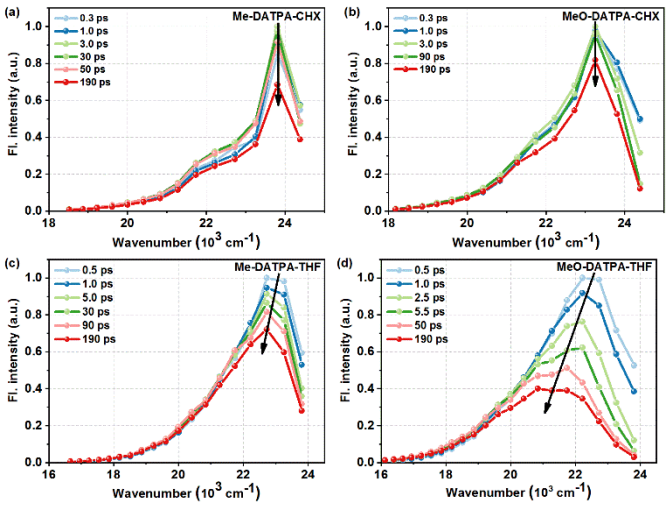

Figure 5. TF spectra recorded at different time delays of **Me- DATPA** (a) and **MeO-DATPA** (b) in CHX and **Me- DATPA** (c) and **MeO-DATPA** (d) in THF.

constant of solvent- induced conformational relaxation process, τ_2 is the lifetime of the relaxed S_1 state and τ_3 is the time constant of intersystem crossing. However, a red shift of SE band in TA spectra is not only ascribed to symmetry breaking process, but also due to the stabilization of a quadrupolar state by solvation. To further confirm the symmetry breaking process, femtosecond TF measurements were performed.

Femtosecond TF measurements

Femtosecond TF measurements were conducted for the two molecules in CHX and THF. The spectra from sub-picosecond to 190 ps are displayed in Figure 5. The evolution trend of TF spectra for the two molecules are similar in CHX, and their intensity and spectral shape are almost unchanged within 50 ps after excitation. For the two molecules in THF, a red-shift of the emission band takes place and the overall fluorescence intensity drops in a few picoseconds time scale. Relative to **Me-DATPA**, it is obvious that the **MeO-DATPA** shows larger red-shift and faster decrease in intensity, and the emission band also becomes broader along with time delays. In order to quantify the evolution of the fluorescence spectra, the spectral peak position and the total fluorescence intensity against with time delays within 30 ps were plotted as shown in Figure 6.

As shown in Figure 6a, in CHX, the fluorescence intensity kinetics of the two molecules are almost similar, consisting of a fast increase during the first several picoseconds then slow decay until about 30 ps. In THF, the total fluorescence intensity of **MeO-DATPA** shows more significant change than that of the **Me-** analogue. For **MeO-DATPA** in THF, the fluorescence intensity loses 40% of its initial intensity in the first 30 ps, which may result from the symmetry broken at the relaxed emissive S_1 state leading to a lower emission dipole moment. For **Me-DATPA**, however, only 10% of its magnitude of fluorescence intensity is lost. Besides, the red-shift of the emission peak is more remarkable for **MeO-DATPA** than that for **Me-DATPA** in THF as shown in Figure 6b. This should be related to a smaller extent of symmetry breaking due to the weak electron-donating strength of methyl group.

To further clarify the symmetry broken kinetics, the temporal evolution of μ_{em} was determined. Figure 7 shows the kinetics of instantaneous emission dipole moments of **Me-** and **MeO-DATPA** in CHX and THF. In addition, the absolute emission dipole moment in the FC state can be calculated through the kinetics of instantaneous emission dipole moment shown in Table 1. For **Me-DATPA** and **MeO-DATPA** in CHX, the μ_{em} of **Me-** and **MeO-DATP**A in the FC state are calculated to be 12.1 D and 11.6 D, respectively, which are similar to those in the

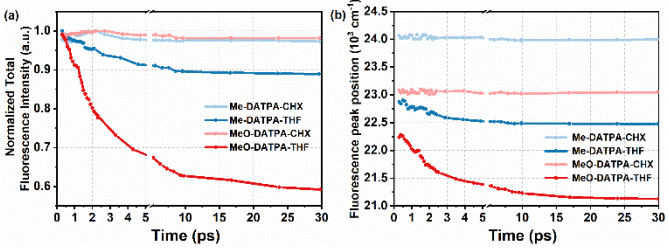

Figure 6. Kinetics profiles of (a) normalized total fluorescence intensity and (b) fluorescence peak position calculated from Gaussian fitting.

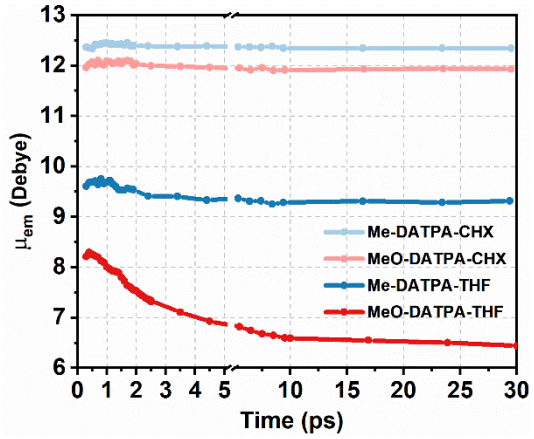

Figure 7. Time dependence of normalized μ_{em} of **Me-** and **MeO-DATPA** in CHX and THF.

relaxed S_1 state. Due to the insensitivity to the nonpolar CHX, the kinetics of μ_{em} of the two molecules show no obvious change with the time delays down to 30 ps, indicating that the excited state always preserve symmetry from the initially formed FC state to the relaxed S_1 state. In THF, the μ_{em} of **MeO-DATPA** is reduced by 25% compared to the initial time during the first 30 ps. The decrease of the instantaneous emission dipole moment is considered as a change in the nature of S_1 state, therefore, the symmetry of the relaxed S_1 state is broken because of solvation. While the μ_{em} of **Me-DATPA** only loses about 5% of its magnitude, which can be explained by a smaller extent of symmetry breaking due to the weaker electron-donating effect with respect to **MeO-** analogue. Besides, the μ_{em} of **Me-** and **MeO-DATPAs** in the FC state are calculated to be 9.6 D and 8.2 D, respectively, which are lower than those in CHX. This indicates that the initially formed electronic state induced by FC excitation in THF has been affected by the solvent field, in other words, the FC state of the two molecules in THF already exhibits a certain extent of dipolar character, and then evolves to an asymmetry S_1 state.

These results indicate that the two quadrupolar molecules show more dipolar character in the more polar solvent environment, while the decrease of μ_{em} is a direct evidence of symmetry breaking. In addition, the larger amplitude of the decreased emission dipole moment of **MeO-DATPA** in THF as compared to that of **Me-DATPA**, indicates that the stronger electron-donating group confers more dipolar characteristics on **MeO-DATPA** in the excited state.[42, 43]

Solvent-induced symmetry breaking processes

In combination with the above-mentioned results, the solvent-induced SBCT mechanism can be summarized as follows as shown in Figure 8. In nonpolar CHX, the solvent fields perceived by two branches are equally weak, therefore, the symmetry of the S_1 state is preserved because excitation delocalized over the whole molecule. In THF, however, because of the solvent fluctuation, the solvent fields around both branches are asymmetric after excitation. This asymmetry field leads to an asymmetry excitation distribution around the two branches, and thus, the quadrupolar molecule loses its high symmetry in the S_1 state, and behaves as a dipole molecule. For **MeO-DATPA**

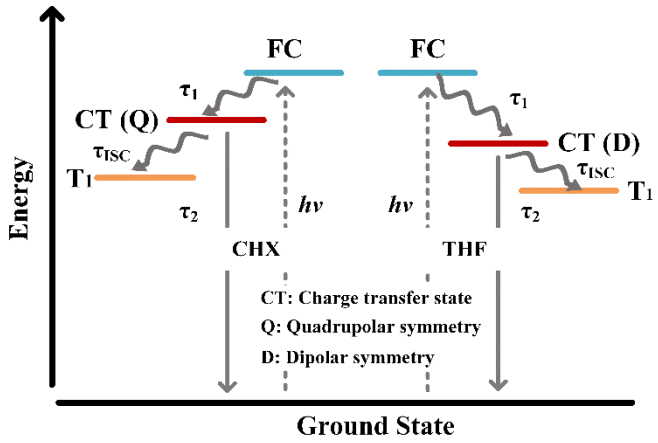

Figure 8. Target evolution models used in global analysis of **Me-DATPA** and **MeO-DATPA** in different solvents.

containing a stronger electron-donating methoxy group, the larger red-shifts of static emission bands and the pronounced decline in k_{nr} indicates that more dipolar characteristic exist in the relaxed S_1 state in polar solvents. As a result, the stronger dipolar solute further polarizes the polar solvent, leading to a more asymmetric solvent field. As a consequence, the extent of symmetry breaking is larger. Furthermore, from the kinetics profiles of the emission dipole moments of **Me-** and **MeO-DATPA** in THF as shown in Figure 7, the decay traces of emission dipole moments of **Me-DATPA** and **MeO-DATPA** in THF are well fitted by a single exponential function with time constants of 2.6 ps and 2.8 ps, respectively. These time constants are close to the time scale indicated by the time constants of solvent-induced conformational relaxation obtained by the TA spectra of **Me-DATPA** (~3.2ps) and **MeO-DATPA** (~2.8ps) in THF. The decay times of emission dipole moments are slightly longer than those reported solvation times in THF,[58] which indicate that conformational relaxations are included in the symmetry breaking process. Solvation causes an asymmetric electronic distribution during conformational relaxation. Therefore, the conformational relaxation plays a significant role in the symmetry breaking process, though is not the origin of symmetry breaking.[40]

Conclusion

In conclusion, we have determined solvation-induced SBCT dynamics of D-π-A-π-D type quadrupolar molecules by steady-state, fs-TA, and fs-TF spectroscopy. Steady-state fluorescence spectra show a clear fluorescence solvatochromism indicating the formation of an asymmetric S_1 state in polar solvent. Through the fs-TA and fs-TF spectral analysis, especially the kinetics of transient emission dipole moment, the solvent-induced symmetry breaking processes are tracked in real-time. In nonpolar CHX, the quadrupolar molecules both preserved their symmetry in the vibrational-related structural relaxed S_1 state. In polar solvent THF, we demonstrated that both molecules experienced symmetry breaking process in the excited state because of strong solvation, while the extent of symmetry breaking is modulated by the different electron-donating functional groups. The molecule with stronger electron-donating group will confer a larger extent of symmetry breaking in D-A-D-type molecules upon excitation. These findings might guide further research intended to a deeper understanding of solute-solvent interaction, especially for the symmetry breaking mechanism in multi-branches molecules.

Conflicts of interest

There are no conflicts to declare.

Acknowledgements

This work was supported by NSFCs (Nos. 21827803, 21773252, 21673252), and the Project for high-grade, precision and advance in Beijing. We also thank the Engineering and Physical Sciences Research Council (EPSRC) APEX project for financial support.

Notes and references

1. R. T. Cheriya, A. R. Mallia and M. Hariharan, *Energy & Environmental Science*, 2014, **7**, 1661-1669.
2. S. Ji, J. Yang, Q. Yang, S. Liu, M. Chen and J. Zhao, *J. Org. Chem.*, 2009, **74**, 4855-4865.
3. A. Mikhaylov, M. Uudsemaa, A. Trummal, E. Arias, I. Moggio, R. Ziolo, T. M. Cooper and A. Rebane, *J. Phys. Chem. Lett.*, 2018, **9**, 1893-1899.
4. H. G. Ryu, M. F. Mayther, J. Tamayo, C. Azarias, E. M. Espinoza, M. Banasiewicz, L. G. Lukasiewicz, Y. M. Poronik, A. Jezewski, J. Clark, J. B. Derr, K. H. Ahn, D. T. Gryko, D. Jacquemin and V. I. Vullev, *J. Phys. Chem. C*, 2018, **122**, 13424-13434.
5. K. Seintis, D. Agathangelou, D. Cvejn, N. Almonasy, F. Bures, V. Giannetas and M. Fakis, *Phys. Chem. Chem. Phys.*, 2017, **19**, 16485-16497.
6. S. Lee and D. Kim, *J. Phys. Chem. A*, 2016, **120**, 9217-9223.
7. H. Meier, Z.-S. Huang and D. Cao, *J. Mater. Chem. C*, 2017, **5**, 9828-9837.
8. H. Kim, B. Keller, R. Ho-Wu, N. Abeyasinghe, R. J. Vazquez, T. Goodson, III and P. M. Zimmerman, *J. Am. Chem. Soc.*, 2018, **140**, 7760-7763.
9. J. Xia, E. Busby, S. N. Sanders, C. Tung, A. Cacciuto, M. Y. Sfeir and L. M. Campos, *Acs Nano*, 2017, **11**, 4593-4598.
10. H. Zhu, W. Li, Y. Wu, B. Liu, S. Zhu, X. Li, H. Agren and W. Zhu, *ACS Sustainable Chem. Eng.*, 2014, **2**, 1026-1034.
11. Y. Li, T. Liu, H. Liu, M.-Z. Tian and Y. Li, *Acc. Chem. Res.*, 2014, **47**, 1186-1198.
12. S. G. Bairu, E. Mghanga, J. Hasan, S. Kola, V. J. Rao, K. Bhanuprakash, L. Giribabu, G. P. Wiederrecht, R. da Silva, L. G. C. Rego and G. Ramakrishna, *J. Phys. Chem. C*, 2013, **117**, 4824-4835.
13. H. Y. Woo, B. Liu, B. Kohler, D. Korystov, A. Mikhailovsky and G. C. Bazan, *J. Am. Chem. Soc.*, 2005, **127**, 14721-14729.
14. B. E. Hardin, H. J. Snaith and M. D. McGehee, *Nat. Photonics*, 2012, **6**, 162-169.
15. Y. Ooyama, A. Matsugasako, K. Oka, T. Nagano, M. Sumomogi, K. Komaguchi, I. Imae and Y. Harima, *Chem. Commun.*, 2011, **47**, 4448-4450.

16. A. Purc, E. M. Espinoza, R. Nazir, J. J. Romero, K. Skonieczny, A. Jezewski, J. M. Larsen, D. T. Gryko and V. I. Vullev, *J. Am. Chem. Soc.*, 2016, **138**, 12826-12832.
17. Z. Kuang, Q. Guo, X. Wang, H. Song, M. Maroncelli and A. Xia, *J. Phys. Chem. Lett.*, 2018, **9**, 4174-4181.
18. H. Song, K. Wang, Z. Kuang, Y. S. Zhao, Q. Guo and A. Xia, *Phys. Chem. Chem. Phys.*, 2019, **21**, 3894-3902.
19. S. Easwaramoorthi, P. Thamaraiselvi, K. Duraimurugan, A. J. Beneto, A. Siva and B. U. Nair, *Chem. Commun.*, 2014, **50**, 6902-6905.
20. B. Carlotti, E. Benassi, A. Spalletti, C. G. Fortuna, F. Elisei and V. Barone, *Phys. Chem. Chem. Phys.*, 2014, **16**, 13984-13994.
21. B. Carlotti, A. Cesaretti, P. L. Gentili, A. Marrocchi, F. Elisei and A. Spalletti, *Phys. Chem. Chem. Phys.*, 2016, **18**, 23389-23399.
22. C. Trinh, K. Kirlikovali, S. Das, M. E. Ener, H. B. Gray, P. Djurovich, S. E. Bradforth and M. E. Thompson, *J. Phys. Chem. C*, 2014, **118**, 21834-21845.
23. S. Das, W. G. Thornbury, A. N. Bartynski, M. E. Thompson and S. E. Bradforth, *J. Phys. Chem. Lett.*, 2018, **9**, 3264-3270.
24. L. G. Lukasiewicz, H. G. Ryu, A. Mikhaylov, C. Azarias, M. Banasiewicz, B. Kozankiewicz, K. H. Ahn, D. Jacquemin, A. Rebane and D. T. Gryko, *Chem. – Asian J.*, 2017, **12**, 1736-1748.
25. C. Sissa, F. Terenziani, A. Painelli, R. B. K. Siram and S. Patil, *J. Phys. Chem. B*, 2012, **116**, 4959-4966.
26. M. Tasior, K. Hassanein, L. M. Mazur, I. Sakellari, D. Gray, M. Farsari, M. Samoc, F. Santoro, B. Ventura and D. T. Gryko, *Phys. Chem. Chem. Phys.*, 2018, **20**, 22260-22271.
27. N. Dozova, L. Ventelon, G. Clermont, M. Blanchard-Desce and P. Plaza, *Chem. Phys. Lett.*, 2016, **664**, 56-62.
28. S. Amthor, C. Lambert, S. Dummler, I. Fischer and J. Schelter, *J. Phys. Chem. A*, 2006, **110**, 5204-5214.
29. Z. Kuang, H. Song, Y. Guo, Q. Guo and A. Xia, *Chin. J. Chem. Phys.*, 2019, **32**, 59-66.
30. T. Kim, J. Kim, H. Mori, S. Park, M. Lim, A. Osuka and D. Kim, *Phys. Chem. Chem. Phys.*, 2017, **19**, 13970-13977.
31. F. Terenziani, A. Painelli, C. Katan, M. Charlot and M. Blanchard-Desce, *J. Am. Chem. Soc.*, 2006, **128**, 15742-15755.
32. Y. Sonoda, *J. Lumin.*, 2017, **187**, 352-359.
33. C. Schierl, W. Alex, L. M. Mateo, B. Ballesteros, D. Shimizu, A. Osuka, T. Torres, D. M. Guldi and G. Bottari, *Angew. Chem. Int. Ed.*, 2019, **58**, 14644-14652.
34. A. Rebane, M. Drobizhev, N. S. Makarov, G. Wicks, P. Wnuk, Y. Stepanenko, J. E. Haley, D. M. Krein, J. L. Fore, A. R. Burke, J. E. Slagle, D. G. McLean and T. M. Cooper, *J. Phys. Chem. A*, 2014, **118**, 3749-3759.
35. B. Dereka and E. Vauthey, *J. Phys. Chem. Lett.*, 2017, **8**, 3927-3932.
36. M. Soderberg, B. Dereka, A. Marrocchi, B. Carlotti and E. Vauthey, *J. Phys. Chem. Lett.*, 2019, **10**, 2944-2948.
37. W. Kim, J. Sung, M. Grzybowski, D. T. Gryko and D. Kim, *J. Phys. Chem. Lett.*, 2016, **7**, 3060-3066.
38. C. Lee, C. H. Choi and T. Joo, *Phys. Chem. Chem. Phys.*, 2020, **22**, 1115-1121.
39. B. Dereka, A. Rosspeintner, M. Krzeszewski, D. T. Gryko and E. Vauthey, *Angew. Chem. Int. Ed.*, 2016, **55**, 15624-15628.
40. B. Dereka, A. Rosspeintner, Z. Li, R. Liska and E. Vauthey, *J. Am. Chem. Soc.*, 2016, **138**, 4643-4649.
41. M. Planells, A. Abate, D. J. Hollman, S. D. Stranks, V. Bharti, J. Gaur, D. Mohanty, S. Chand, H. J. Snaith and N. Robertson, *J. Mater. Chem. A*, 2013, **1**, 6949-6960.
42. T. Kim, W. Kim, H. Mori, A. Osuka and D. Kim, *J. Phys. Chem. C*, 2018, **122**, 19409-19415.
43. J. S. Beckwith, A. Rosspeintner, G. Licari, M. Lunzer, B. Holzer, J. Froehlich and E. Vauthey, *J. Phys. Chem. Lett.*, 2017, **8**, 5878-5883.
44. C. J. Jamorski and M. E. Casida, *J. Phys. Chem. B*, 2004, **108**, 7132-7141.
45. C. Peltier, C. Adamo, P. P. Laine, S. Campagna, F. Puntoriero and I. Ciofini, *J. Phys. Chem. A*, 2010, **114**, 8434-8443.
46. M. Savarese, A. Aliberti, I. De Santo, E. Battista, F. Causa, P. A. Netti and N. Rega, *J. Phys. Chem. A*, 2012, **116**, 7491-7497.
47. A. D. Bani-Yaseen and M. Al-Balawi, *Phys. Chem. Chem. Phys.*, 2014, **16**, 15519-15526.
48. A. M. Brouwer, *Pure Appl. Chem.*, 2011, **83**, 2213-2228.
49. Z. Kuang, G. He, H. Song, X. Wang, Z. Hu, H. Sun, Y. Wan, Q. Guo and A. Xia, *J. Phys. Chem. C*, 2018, **122**, 3727-3737.
50. M. Zhou, S. Vdovic, S. Long, M. Zhu, L. Yan, Y. Wang, Y. Niu, X. Wang, Q. Guo, R. Jin and A. Xia, *J. Phys. Chem. A*, 2013, **117**, 10294-10303.
51. J. J. Snellenburg, S. P. Laptenok, R. Seger, K. M. Mullen and I. H. M. van Stokkum, *J. Stat. Softw.*, 2012, **49**, 1-22.
52. I. H. M. van Stokkum, D. S. Larsen and R. van Grondelle, *Biochim. Biophys. Acta, Bioenerg.*, 2004, **1657**, 82-104.
53. M. J. T. Frisch, G. W.; Schlegel, H. B.; Scuseria, G. E.;, M. A. C. Robb, J. R.; Scalmani, G.; Barone, V.; Mennucci, and G. A. B.; Petersson, et al.. 2013, **Gaussian, Inc., Wallingford CT.**
54. T. Yanai, D. P. Tew and N. C. Handy, *Chem. Phys. Lett.*, 2004, **393**, 51-57.
55. C. A. Jimenez-Hoyos, B. G. Janesko and G. E. Scuseria, *Phys. Chem. Chem. Phys.*, 2008, **10**, 6621-6629.
56. H. Zhu, Y. Li, J. Chen, M. Zhou, Y. Niu, X. Zhang, Q. Guo, S. Wang, G. Yang and A. Xia, *ChemPhysChem*, 2015, **16**, 3893-3901.
57. Y. H. Kim, D. W. Cho, N. W. Song, D. Kim and M. Yoon, *J. Photochem. Photobiol., A*, 1997, **106**, 161-167.
58. M. L. Horng, J. A. Gardecki, A. Papazyan and M. Maroncelli, *J. Phys. Chem.*, 1995, **99**, 17311-17337.
59. J. Herbich and A. Kapturkiewicz, *J. Am. Chem. Soc.*, 1998, **120**, 1014-1029.
60. T. Kumpulainen, B. Lang, A. Rosspeintner and E. Vauthey, *Chem. Rev.*, 2017, **117**, 10826-10939.
61. H. Song, Z. Kuang, X. Wang, Y. Guo, Q. Guo, H. Zhang and A. Xia, *J. Phys. Chem. C*, 2018, **122**, 15108-15117.

TOC Graphic

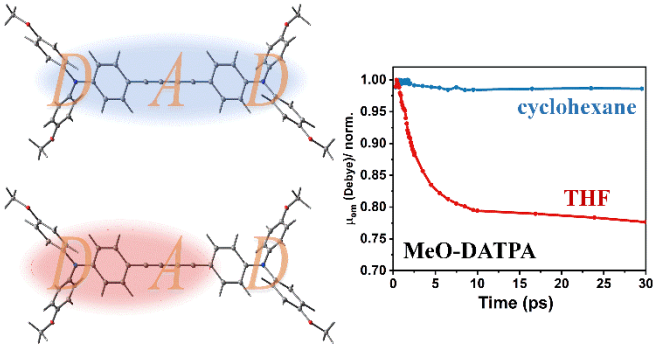

Donor-π-Acceptor-π-Donor quadrupolar dyes with different electron-donating abilities have been chosen to investigate the solvation-dependent excited state dynamics. The solvent-induced symmetry breaking processes are successfully tracked in real-time. The results demonstrated how solvation can fine-tune the photophysical properties of push-pull dyes, and highlighted the importance of the magnitude of symmetry breaking in quadrupolar molecules in the excited state ICT processes.